Floquet stability and Lagrangian statistics of a non-linear time-dependent ABC dynamo

Calum S. Skene[1,*] and Steven M. Tobias[1]

[1]*Department of Applied Mathematics, University of Leeds, Leeds LS2 9JT, UK*

(Dated: January 26, 2023)

Abstract

The Lagrangian statistics of a time-dependent ABC flow are considered, with time-dependence introduced via harmonic oscillation with frequency Ω. By calculating the finite-time Lyapunov exponents (FTLEs), the Lagrangian statistics of the system are determined for a range of values of Ω. These statistics are calculated for the kinematic regime where the flow remains an ABC flow, the non-linear regime with dynamo action present, and a second hydrodynamic state reached through instability of the original ABC flow. It is found that there are significant differences between these three states, with most cases showing a decrease in their FTLEs as the flow deviates from its original ABC form. Furthermore, these changes are highly dependent on Ω, with lower frequencies leading to higher FTLEs in the non-linear regime, and unstable regimes. By examining the Lagrangian statistics with respect to the dynamo behaviour observed, we discuss their potential relevance to non-linear saturation, self-killing dynamos, and the importance of the initial hydrodynamic state. The numerical code developed for this project is also available.

I. INTRODUCTION

In an electrically conducting fluid, the coupling between the velocity field and magnetic field can lead to a self-sustaining magnetic field. This phenomena is termed dynamo action, and is an important physical process underpinning the behaviour of many astrophysical flows [1]. The Lagrangian properties of dynamo flows have been conjectured to play a key role in the kinematic and dynamic properties of dynamo action; certainly this is the case in the kinematic regime at asymptotically high magnetic Reynolds number (R_m) — the so-called fast dynamo problem. Dynamical systems theory applied to fast dynamo action demonstrates that the topological entropy of the flow bounds the asymptotic growth-rate of the dynamo [2]; see also [3]. This rules out the possibility of fast dynamo action for integrable flows and shows that chaotic particle paths are required for a flow to be a fast dynamo.

These results have led to a sustained interest in the Lagrangian properties of saturated dynamo flows. It is an interesting question as to what can be determined about the mechanism for dynamo saturation from a consideration of the Lagrangian statistics. Since growth of a magnetic field relies on stretching overcoming the dissipative action of magnetic diffusion, it could be that dynamos saturate (and become statistically marginal) in the nonlinear regime by either reducing the stretching (which would be manifested as a suppression of the chaos in the high R_m limit), enhancing the

* Corresponding Author: c.s.skene@leeds.ac.uk

diffusion or a combination of the two. How the magnetic field might act so as to reduce the stretching is undetermined. It might be that the field acts so as to reduce the amplitude of dynamo flow back to the marginal state — i.e. the flow amplitude might be reduced so that $R_m \approx R_{m,c}$ for dynamo action. This drastic intervention of the flow seems unlikely at high R_m (as argued in Cattaneo and Tobias [4]). More likely is that the field acts to reduce the amplitude of the flow somewhat, but also suppresses its stretching properties in a subtle manner [5].

This suppression of chaos was shown to be important in a simplified 2.5 dimensional dynamo — here a 2.5-dimensional flow is one that has all three components of the velocity but each component only depends on two spatial coordinates. In order to maintain two-dimensionality in the nonlinear regime, the Lorentz force was projected back onto the z-invariant velocity [5]. However firm conclusions for models that include the full Lorentz force in three-dimensions are much more difficult to draw. A variety of investigations have been carried out on the Lagrangian properties of saturated dynamo states, for a variety of driving mechanisms; not all of these have included a description of the stretching as measured by the Lyapunov exponents.

Zienicke *et al.* [6] considered a forcing based on the steady ABC flow at moderate scale. This flow, with standard parameters is known to be weakly chaotic; however at high Re this flow goes unstable to a flow with a range of spatial scales and complicated time dependence. At moderate Reynolds number (Re) and R_m they found that the growth of a large-scale field can excite velocity modes that can lead to the mean Lyapunov exponents of the saturated state being much larger than that of the kinematic flow, as the flow has many more excited modes in the nonlinear state.

Rempel *et al.* [7] considered the Lagrangian properties of the velocity field of a helical MHD dynamo, with moderate scale, steady forcing. In addition to computing the Lagrangian coherent structures (LCS), they also calculated the statistics of the finite-time Lyapunov exponents (FTLEs) and showed that these decay as a linear function of magnetic energy of the saturated dynamo.

Homann *et al.* [8] considered dynamo action in a forced Taylor–Green system and analysed the statistical properties of both the velocity and magnetic fields in Eulerian and Lagrangian frameworks. They found that these statistics are changed between the kinematic and saturated regimes, with the saturated trajectories aligning more with the mean magnetic field and the probability density functions (PDFs) of the magnetic field changing to quasi-Gaussian. Moreover they observed a dramatic increase of the correlation time of the velocity and magnetic fields in the saturated regime. However, for this flow, the stretching properties as given by the FTLEs remained unmeasured.

Of particular relevance to our study is that of Brummell *et al.* [9], who consider an ABC-flow with an added harmonic time dependence which oscillates the ABC flow along the line $x = y = z$.

By introducing this time-dependence the chaotic nature of the original ABC flow is enhanced, with the time-dependent flow showing decreased areas of integrability. The degree of chaos induced in the flow depends on the frequency of the oscillation of the imposed flow (or forcing) [see also 10].

This is confirmed by considering the FTLEs of the flow. It is shown that this added chaos aids kinematic dynamo action, with the time-dependent ABC flow showing stronger growth rates, as well as behaving as a 'quick' dynamo. Their study also considers the non-linear regime by performing simulations of the coupled Navier–Stokes and induction equations, where the ABC flow is initially sustained by a body forcing. Although in all cases the flow is a kinematic dynamo, for some frequencies of the oscillations the dynamo is not sustained in the non-linear regime, and decays until only a turbulent hydrodynamic stated termed U_1 is left. Note that this secondary hydrodynamic state can also be reached through hydrodynamic instability of the original ABC-flow.

Our current study builds upon the work of Brummell *et al.* [9] through calculating the FTLEs of the flow in both the non-linear regime where the Lorentz force is saturating the dynamo, and also for the flow U_1. This involves solving the coupled Navier–Stokes and induction equations together with tracking Lagrangian particles. By calculating the FTLEs in these two flow regimes we hope to further elucidate the dynamics responsible for dynamo-saturation, as well as to explain why some dynamos are unable to sustain themselves in the non-linear regime.

As well as calculating the FTLEs, we also consider the Floquet stability [11] of the time-dependent ABC-flow to both hydrodynamic and magnetic perturbations. In this manner, all the unstable directions of the original flow together with their growth rates can be systematically captured. The paper proceeds as follows; §II outlines the mathematical and numerical setup, containing the details of the governing equations, Floquet stability analysis, and finite-time Lyapunov exponents. The results are then presented in §III, with conclusions subsequently being offered in §IV.

II. MATHEMATICAL AND NUMERICAL SETUP

A. Formulation: Governing equations and Numerical Methods

The system is governed by the magnetic induction and Navier–Stokes equations, which in non-dimensional form are

$$(\partial_t - R_m^{-1}\nabla^2)\boldsymbol{B} = \nabla \times (\boldsymbol{U} \times \boldsymbol{B}), \tag{1}$$

$$(\partial_t - Re^{-1}\nabla^2)\boldsymbol{U} + \boldsymbol{U} \cdot \nabla \boldsymbol{U} = -\nabla p + \boldsymbol{J} \times \boldsymbol{B} + \boldsymbol{F}, \tag{2}$$

$$\nabla \cdot \boldsymbol{U} = \nabla \cdot \boldsymbol{B} = 0. \tag{3}$$

The non-dimensional variables are the fluid velocity $\boldsymbol{U}$, magnetic field $\boldsymbol{B}$, pressure p, and electric current $\boldsymbol{J} = \nabla \times \boldsymbol{B}$. By non-dimensionalising time with respect to a typical turnover time of the flow (U) and space with respect to the lengthscale of the domain (L), the non-dimensional parameters of Reynolds number $Re = UL/\nu$ and magnetic Reynolds number $R_m = UL/\eta$ have been introduced. Moreover in this non-dimensionalisation the field is measured in units of the Alfvén speed. The domain is taken to be $(x, y, z) \in [0, 2\pi]^3$ with periodic boundary conditions. Following Brummell *et al.* [9], the external (Re-dependent) forcing term $\boldsymbol{F}$ is chosen such that in the absence of magnetic field there exists an order unity solution for the velocity field $\boldsymbol{U}_0$ given by

$$\begin{aligned}\boldsymbol{U}_0 = (&\sin(z + \epsilon \sin(\Omega t)) + \cos(y + \epsilon \sin(\Omega t)),\\ &\sin(x + \epsilon \sin(\Omega t)) + \cos(z + \epsilon \sin(\Omega t)),\\ &\sin(y + \epsilon \sin(\Omega t)) + \cos(x + \epsilon \sin(\Omega t))).\end{aligned} \tag{4}$$

For $\epsilon = 0$ this flow corresponds to an ABC flow with $A = B = C = 1$. However, by varying ϵ, the flow is allowed to 'wobble' around the ABC state with amplitude ϵ and angular frequency Ω. The initial kinetic energy density is displayed in figure 1, showing that it has large scale structures. For low Re this flow is hydrodynamically stable.

To solve this system numerically we first replace the magnetic induction equation for $\boldsymbol{B}$ with an equation for the magnetic vector potential $\boldsymbol{A}$ defined such that $\boldsymbol{B} = \nabla \times \boldsymbol{A}$ and with $\boldsymbol{A}$ taken to satisfy the Coulomb gauge condition $\nabla \cdot \boldsymbol{A} = 0$. The resulting system is solved numerically using spectral methods via the open-source PDE solver Dedalus [12]. A resolution of $96 \times 96 \times 96$ is used for all dynamo calculations when particles are not being tracked (see the next section), to ensure that the resolution is high enough to prevent spurious dynamo solutions [13]. Two-thirds dealiasing is used to treat all non-linear terms.

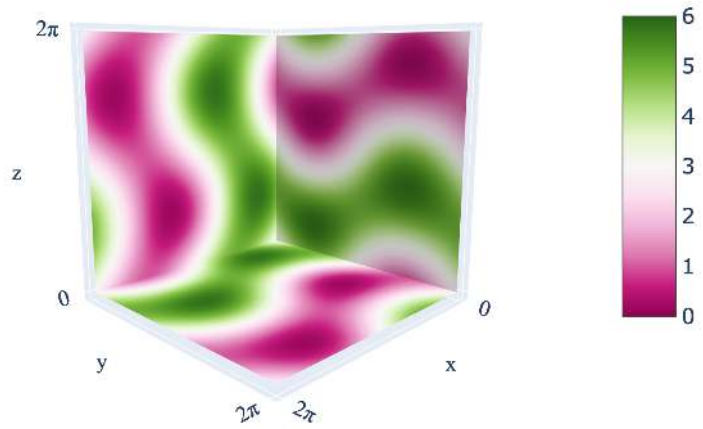

FIG. 1: Contour plot of the initial kinetic energy density connected with $\boldsymbol{U}_0$.

B. Floquet stability analysis

The hydrodynamic state $\boldsymbol{q}_0 = (\boldsymbol{B}, \boldsymbol{U}, p)^T = (\boldsymbol{0}, \boldsymbol{U}_0, P_0)^T$, (with P_0 found through rearrangement of the momentum equation) is an exact periodic solution to equations (1)-(3). Therefore, the stability of the periodic solution $\boldsymbol{q}_0$ to perturbations can be found via a Floquet stability analysis [11] (though traditionally the stability of such flows to dynamo action has usually been found by timestepping). To this end, we first rewrite equations (1)-(3) in the more general form

$$\boldsymbol{M}\frac{\partial \boldsymbol{q}}{\partial t} = \boldsymbol{\mathcal{N}}(\boldsymbol{q}, \boldsymbol{F}), \tag{5}$$

where the matrix $\boldsymbol{M}$ ensures there is no time-derivative term in the continuity equation, and the operator $\boldsymbol{\mathcal{N}}$ represents the right hand side of the equations. We then linearise these equations about $\boldsymbol{q}_0$ to give the linearised equations

$$\boldsymbol{M}\frac{\partial \boldsymbol{q}'}{\partial t} = \boldsymbol{A}(t)\boldsymbol{q}', \tag{6}$$

where

$$\boldsymbol{A}(t) = \left.\frac{\partial \boldsymbol{\mathcal{N}}}{\partial \boldsymbol{q}}\right|_{\boldsymbol{q}=\boldsymbol{q}_0(t)}. \tag{7}$$

As equation (6) is linear, the solution at any time t can be obtained from an initial condition at time t_0 using the state-transition matrix $\boldsymbol{\Psi}(t, t_0)$, via $\boldsymbol{q}'(t) = \boldsymbol{\Psi}(t, t_0)\boldsymbol{q}'(t_0)$. The matrix $\boldsymbol{\Psi}(t_0 + T, t_0)$ that propagates a state forward by one period T is known as the monodromy matrix. By taking the eigenvalue decomposition of this matrix, i.e. by solving $\boldsymbol{\Psi}(t_0 + T, t_0)\boldsymbol{q}_i(t_0) = \mu_i \boldsymbol{q}_i(t_0)$, we can write

any perturbation in terms of the decomposition as

$$\boldsymbol{q}' = \sum_i \boldsymbol{q}_i \exp(t\lambda_i), \tag{8}$$

where $\lambda_i = \log(\mu_i)/T$. The stability of the flow can then be determined from the Floquet multipliers μ_i, with the flow stable if $|\mu_i| < 1$ and unstable if $|\mu_i| > 1$.

Our linearised equations (6) can be written as

$$(\partial_t - Re^{-1}\nabla^2)\boldsymbol{U}' + \boldsymbol{U}_0 \cdot \nabla \boldsymbol{U}' + \boldsymbol{U}' \cdot \nabla \boldsymbol{U}_0 = -\nabla p', \tag{9}$$

$$\nabla \cdot \boldsymbol{U}' = 0, \tag{10}$$

$$(\partial_t - R_m^{-1}\nabla^2)\boldsymbol{B}' = \nabla \times (\boldsymbol{U}_0 \times \boldsymbol{B}'), \tag{11}$$

$$\nabla \cdot \boldsymbol{B}' = 0. \tag{12}$$

This shows that equation (6) can be decoupled into two Floquet stability analyses; one for the hydrodynamic stability obtained through solving (9) and (10), and another for the stability of the magnetic field through solving (11) and (12). In other words, the hydrodynamic stability of the $\boldsymbol{U}_0$ flow is independent from the stability of the magnetic field. Hence we should expect that, in the kinematic regime, perturbations to the velocity and magnetic fields will grow independently of each other in accordance with their Floquet multipliers. It is important to note that, this is the case only for a hydrodynamic basic state; decoupling would not occur for the Floquet stability of an MHD basic state. Although Floquet analysis around a periodic MHD state is also possible, and would be relevant to the instability of saturated dynamo solutions to long wavelength instabilities, this is beyond the scope of our current study.

Numerically we solve the hydrodynamic and magnetic stability problems separately following the method discussed by Barkley and Henderson [14]. For the hydrodynamic stability problem we let the state transition matrix for the linear problem given by (9) and (10) be denoted by $\boldsymbol{\Psi}_U$. The action of $\boldsymbol{\Psi}_U(T)$ on a vector $\boldsymbol{a}$ is then provided in a matrix-free manner by solving equations (9) and (10) with initial condition $\boldsymbol{U}' = \boldsymbol{a}$ over one period $T = 2\pi/\Omega$. The eigenvalues of $\boldsymbol{\Psi}_U(T)$ can then be found from this matrix-free operation using an eigenvalue solver, yielding the Floquet multipliers and modes. The magnetic stability problem is solved using the same procedure with equations (11) and (12).

C. Finite-time Lyapunov exponents

As noted in the introduction, information about the degree of stretching in the flow can be gained by calculating the distribution of finite-time Lyapunov exponents (FTLEs) In order to calculate

these, we follow the algorithm of Soward [15] (see also [16]) and consider tracking a set of particles that are passively advected by the fluid. Taking N particles with positions $\{\boldsymbol{p}_i\}_{i=0}^{N-1}$ we track the particles by solving

$$\frac{\mathrm{d}}{\mathrm{d}t}\boldsymbol{p}_i = \boldsymbol{U}(\boldsymbol{p}). \tag{13}$$

Letting $\mathcal{S}$ denote the fluid velocity gradient tensor with $\mathcal{S}(\boldsymbol{p}) = \nabla_{\boldsymbol{x}=\boldsymbol{p}}\boldsymbol{U}$, we also solve

$$\frac{\mathrm{d}}{\mathrm{d}t}\boldsymbol{D} = \boldsymbol{S}(\boldsymbol{p})\boldsymbol{D}, \tag{14}$$

for each particle path starting with $\boldsymbol{D} = \mathrm{diag}(2^{-1/2}, 2^{-1/2}, 0)$. For each time t we form the matrix

$$\boldsymbol{C}(t) = \boldsymbol{D}(t)^T\boldsymbol{D}(t). \tag{15}$$

The FTLE connected to the position $\boldsymbol{x}_0$ is then the slope of $l(t;\boldsymbol{x}_0) = \log(\sum_{i,j}\boldsymbol{C}_{i,j}(t)/2)/2$ where $\boldsymbol{C}$ arises from a particle whose initial position is $\boldsymbol{x}_0$. The slope of the line is found using linear regression.

When calculating the FTLEs we solve the governing equations as described in the previous section, tracking the particles using a particle tracking code for Dedalus developed for this study. For what follows, we will concentrate on the calculation of FTLEs on the plane $z = 0$, i.e. the initial particle positions are taken to be equispaced $(x_i, y_i, 0)$, with the $x - y$ plane consisting of 128×128 particles, and a time horizon of $T = 30$ matching that of Brummell *et al.* [9]. Due to the increased numerical burden of tracking the particles, the resolution is decreased to $64 \times 64 \times 64$ when calculating the FTLEs. However, the initial condition for tracking the particles always comes from the higher resolution results. This, coupled with the fact that the time horizon for the FTLE calculations is small, means that we stay close enough to the high resolution solution whilst keeping the computation feasible. The numerical code for particle tracking in Dedalus v2 and FTLE calculation has been made available as part of the companion code for this paper [17].

D. Passive vector field evolution

A less rigorous, though still informative method for calculating the stretching properties of a flow is to calculate the response of a passive vector field to the flow. Following Cattaneo and Tobias [4] we will also consider the evolution of a passive vector field which satisfies the induction equation but does not couple with the velocity field via a Lorentz force. To this end, we solve equations (1)-(3) together with

$$(\partial_t - R_m^{-1}\nabla^2)\boldsymbol{Z} = \nabla \times (\boldsymbol{U} \times \boldsymbol{Z}), \tag{16}$$

$$\nabla \cdot \boldsymbol{Z} = 0. \tag{17}$$

By tracking $\boldsymbol{Z}$ we are able to see how a magnetic field would behave for the velocity field stemming from a non-linearly saturated dynamo. While it seems that $\boldsymbol{Z}$, which solves the same equation as $\boldsymbol{B}$, must follow the same trajectory as $\boldsymbol{B}$, this is in fact only true if the initial condition for $\boldsymbol{Z}$ is the same as that of $\boldsymbol{B}$. The reason for this is that there is no $\boldsymbol{Z}$-based Lorentz force, meaning that $\boldsymbol{U}$ is independent of $\boldsymbol{Z}$ and that the evolution of $\boldsymbol{Z}$ is completely linear. As no particles are being tracked in this case, the resolution is again set at $96 \times 96 \times 96$. The aim here is to determine how well one can understand the chaotic properties of the flow using this proxy method, which is simpler (and less expensive) computationally than calculating the FTLEs.

III. RESULTS

A. Floquet stability analysis

We begin our results by considering the stability of the periodic state $\boldsymbol{U}_0$, using the procedure outlined in section II B. Again, we stress that around a purely hydrodynamic base-state the hydrodynamic and magnetic stability problems decouple and may be considered separately. Figure 2 shows the Floquet exponents found for the two cases at two representative frequencies. For Floquet exponents λ with $\mathrm{Real}(\lambda) > 0$ there will be an exponential growth of the mode, indicating instability. Hence, exponents above the line $\mathrm{Real}(\lambda) = 0$ indicate unstable directions.

For $Re = R_m = 100$ the flow is, in general, more unstable to magnetic perturbations rather than hydrodynamic perturbations, agreeing with the observations of Brummell *et al.* [9]. However, for $\Omega = 0.5$ this is not the case, and the flow is much more unstable to a hydrodynamic perturbation with $\mathrm{Imag}(\lambda) = 0$, which shows that it is a purely growing instability and has no oscillation frequency associated with it. This is made clearer by considering the maximum growth rate for each frequency, displayed in figure 3.

For verification of our Floquet approach, the results of Brummell *et al.* [9] are added to figure 3b. As we can see there is a good quantitative agreement, with our results bounded above by those of Brummell *et al.* [9]. The reason for this can be attributed to the method used to obtain the growth rates. Ours stem from a single modal structure, whereas those of Brummell *et al.* [9] are obtained via linear regression of the magnetic energy obtained from a simulation, meaning that the superposition of two or more growing modes can give rise to a higher magnetic energy growth rate. Figure 3 also shows the results of the Floquet analysis at $R_m = 120$. As the maximum growth rate does not change significantly, we can postulate that we are in a regime where the growth-rate has

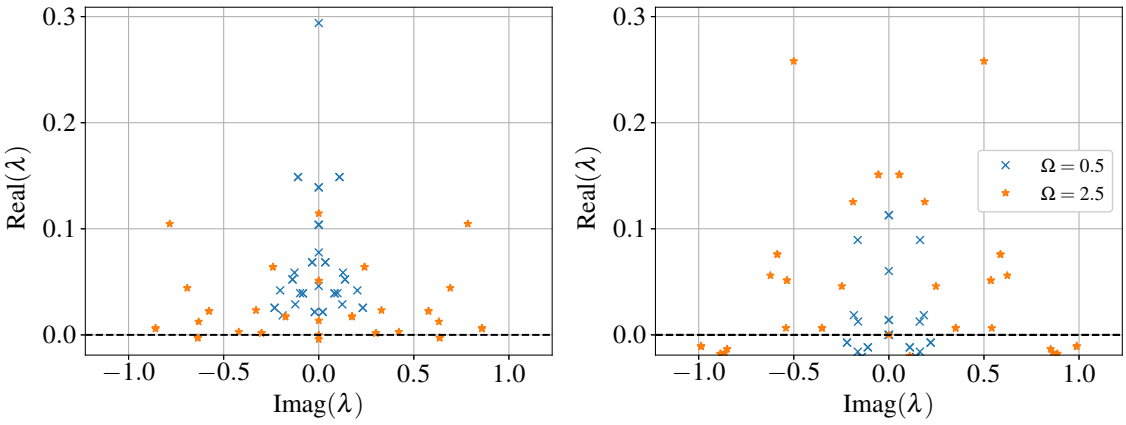

(a) Hydrodynamic Floquet exponents

(b) Magnetic Floquet exponents

FIG. 2: Floquet exponents for $\epsilon = 1$, $Re = R_m = 100$. The stability boundary is shown as a dotted line in each figure.

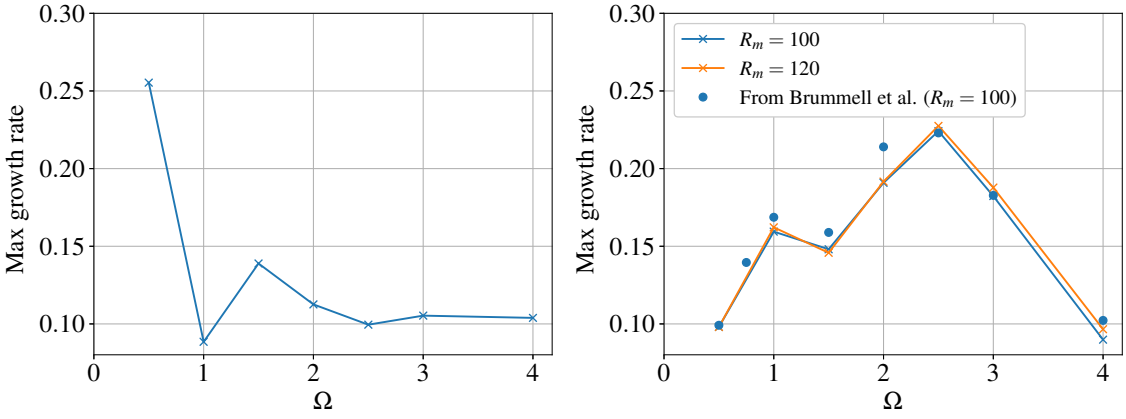

(a) Maximum growth rates for the kinetic energy.

(b) Maximum growth rates for the magnetic energy

FIG. 3: Maximum growth rates for the hydrodynamic and magnetic stability problems.

saturated as a function of R_m; in this sense the time-dependent flows are acting as “quick" dynamos [18]. This asymptotic behaviour is believed to set in at lower magnetic Reynolds numbers for time-varying hydrodynamic states [9, 13], than for steady ABC-flow [19].

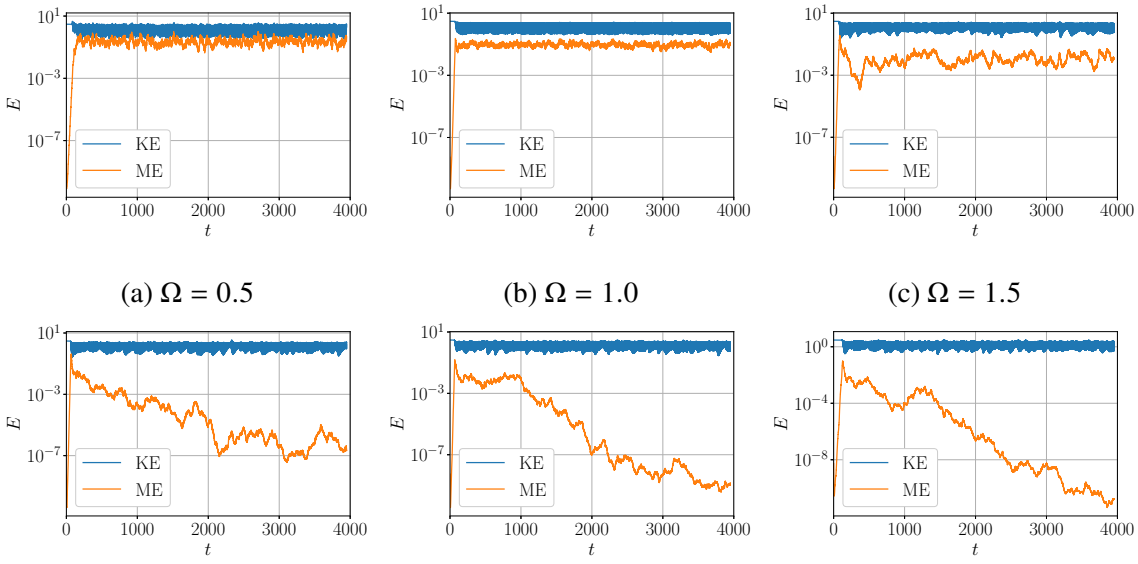

(a) $\Omega = 0.5$ (b) $\Omega = 1.0$ (c) $\Omega = 1.5$

(d) $\Omega = 2.0$ (e) $\Omega = 3.0$ (f) $\Omega = 4.0$

FIG. 4: Kinetic and magnetic energies over time for $\epsilon = 1$ and $Re = R_m = 100$

B. Non-linear evolution

Before considering the FTLEs we first summarise the flow behaviour of an initial state consisting of a small magnetic field and the hydrodynamic state $\boldsymbol{U}_0$. Figure 4 shows the results for $Re = R_m = 100$. We see that for all frequencies there is an initial exponential growth of the magnetic field. This is not surprising as the results of the Floquet analysis show that the flow is unstable to magnetic perturbations. More interesting is the subsequent behaviour. For the considered frequencies $\Omega \leq 1.5$ the magnetic energy saturates, showing that the Lorentz force acts to stabilise the growth of the magnetic field. However, for higher frequencies the magnetic energy eventually decays. This means that the velocity field that results after deviation from its initial $\boldsymbol{U}_0$ form is stable to magnetic perturbations. In this case, the magnetic energy eventually decays to negligible values leaving a purely hydrodynamic state that can be reached from a hydrodynamic simulation via the instability of the base-state to hydrodynamic perturbations. Following Brummell *et al.* [9] we call this secondary state $\boldsymbol{U}_1$.

Repeating this procedure at the higher magnetic Reynolds number of $R_m = 120$ we obtain figure 5. In this case for all frequencies the dynamo saturates leading to a non-linear dynamo solution. As the Floquet analysis revealed that there is so significant change in the stability properties of $\boldsymbol{U}_0$ for $R_m = 120$ the reason behind this saturation must either lie in the stability properties of $\boldsymbol{U}_1$ to

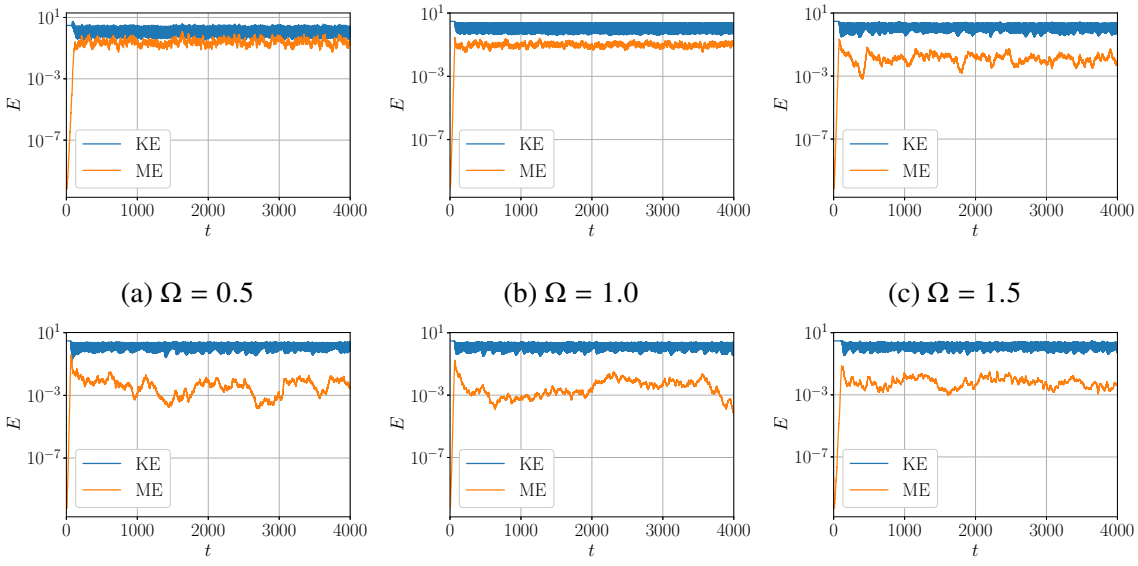

(a) $\Omega = 0.5$ (b) $\Omega = 1.0$ (c) $\Omega = 1.5$

(d) $\Omega = 2.0$ (e) $\Omega = 3.0$ (f) $\Omega = 4.0$

FIG. 5: Kinetic and magnetic energies over time for $\epsilon = 1$, $Re = 100$, and $R_m = 120$ starting from $\boldsymbol{U}_0$.

magnetic perturbations, or in non-linear interactions between the magnetic field and velocity field via the Lorentz force. Hence in order to investigate this we examine the stability properties of $\boldsymbol{U}_1$.

As $\boldsymbol{U}_1$ is not an exact periodic solution of the governing equations, but is instead a quasi-periodic state, we cannot use Floquet theory to determine the behaviour of a small magnetic field. Instead we run a simulation starting from an initial state in the $\boldsymbol{U}_1$ attractor and seed it with a small random magnetic field. The results of this for $R_m = 100$ and $R_m = 120$ are shown in figures 6 and 7, respectively. For $R_m = 100$ figure 6 shows that the frequencies at which the magnetic energy eventually decays are the same frequencies at which $\boldsymbol{U}_1$ is stable to magnetic perturbations. This means that if non-linear effects are unable to alter the velocity field, then the magnetic field will eventually decay with no chance to grow again. For this reason, at $Re = 100$ where the hydrodynamic state $\boldsymbol{U}_0$ is unstable, it is unclear whether these dynamos are 'self-killing' initially through an unfavourable modification of the velocity field via the Lorentz force, or whether they decay through the rise of the stable $\boldsymbol{U}_1$ hydrodynamic state. It is also worth noting that although the other frequencies are unstable to magnetic perturbations, the growth rates are significantly reduced than that obtained for $\boldsymbol{U}_0$, indicating that while $\boldsymbol{U}_1$ is still susceptible to kinematic dynamo action, it is less efficient.

Turning our attention to $R_m = 120$, we see from figure 7 that all frequencies show a positive

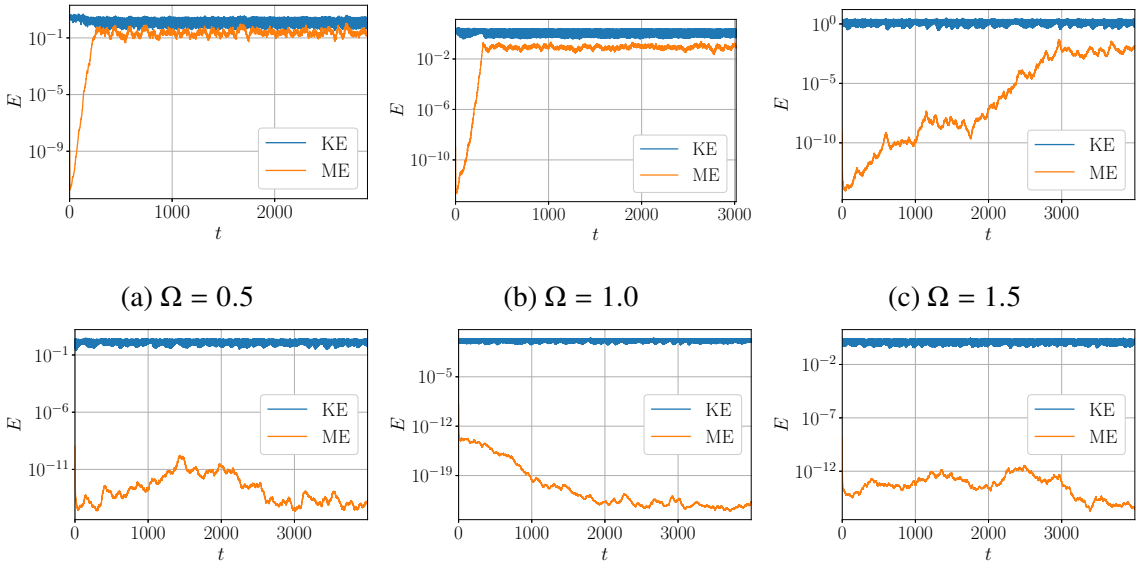

(a) $\Omega = 0.5$ (b) $\Omega = 1.0$ (c) $\Omega = 1.5$

(d) $\Omega = 2.0$ (e) $\Omega = 2.5$ (f) $\Omega = 4.0$

FIG. 6: Kinetic and magnetic energies over time for $\epsilon = 1$ and $R_m = 100$ starting from $\boldsymbol{U}_1$.

growth rate. However, for $\Omega \geq 2$ this growth rate is extremely small, with $\Omega = 2.5$ not rising significantly on a long time-scale. Therefore, on short time scales the flow will appear neutral to magnetic perturbations and we can expect that only a slight non-linear effect via the Lorentz force will be needed in order to saturate the growth of magnetic energy. Again we note that for all frequencies the growth rates for $\boldsymbol{U}_1$ are lower than that of $\boldsymbol{U}_0$.

C. Lagrangian statistics

Now that the non-linear evolution of a magnetic field has been described for a range of parameters, we turn our attention to understanding the growth and saturation of the magnetic field via an examination of the Lagrangian statistics of the flow field. We first seek to verify the particle tracking code with the work of Brummell *et al.* [9]. To this end, we set $Re = 100$, $R_m = 100$, $\epsilon = 1$ and consider a range of values for Ω on the plane $z = 0$. For these parameters the flow field $\boldsymbol{U}$ remains close to $\boldsymbol{U}_0$ despite the exponentially growing magnetic field due to the stability properties of the hydrodynamic state (see section III A). This means that by calculating the FTLEs with a time integration of 30 time-units, we stay within this kinematic regime and our results should match those of Brummell *et al.* [9] for which the $\boldsymbol{U}_0$ flow is imposed.

Figure 8a shows the mean FTLEs calculated with our current approach, and with the results of

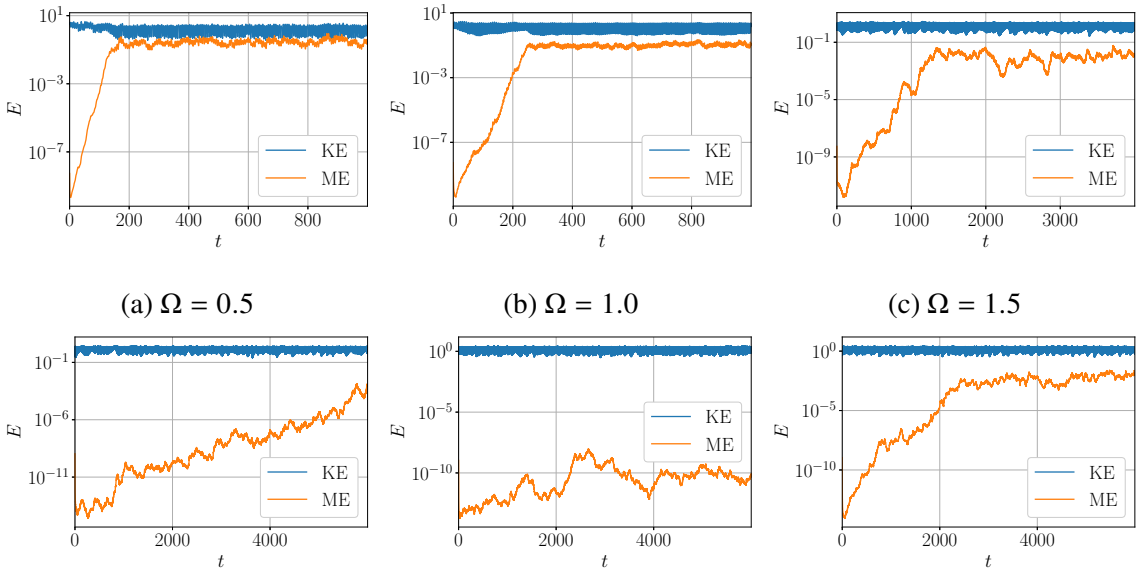

(a) $\Omega = 0.5$ (b) $\Omega = 1.0$ (c) $\Omega = 1.5$

(d) $\Omega = 2.0$ (e) $\Omega = 2.5$ (f) $\Omega = 4.0$

FIG. 7: Kinetic and magnetic energies over time for $\epsilon = 1$ and $R_m = 120$ starting from $\boldsymbol{U}_1$.

Brummell *et al.* [9]. We see that the calculated values show a good agreement, both verifying our approach and showing that the results of Brummell *et al.* [9] hold in the presence of a small, but non-zero, magnetic field. The weak field here has had very little impact on the degree of chaos in the flow. As in [9] we see that there is a qualitative correspondence between the mean FTLEs and the stability properties of $\boldsymbol{U}_0$. Indeed, larger values of the FTLE occur at frequencies for which the magnetic growth rate (shown in figure 3b) are highest.

Having verified our particle tracking approach we now consider calculating the FTLEs for the secondary hydrodynamic state $\boldsymbol{U}_1$. Figure 8b shows that the flow $\boldsymbol{U}_1$ is on average less chaotic than $\boldsymbol{U}_0$ with the FTLEs for most frequencies decreasing. The exception to this is the lowest frequency considered, $\Omega = 0.5$. For this frequency the mean FTLE for $\boldsymbol{U}_1$ is significantly greater than for $\boldsymbol{U}_0$. One possible explanation for this can be obtained by examining the stability of $\boldsymbol{U}_0$ to hydrodynamic perturbations. There are two main reasons for suspecting this link. The first is that there is a correspondence between the maximum growth rates of the kinetic energy (shown in figure 3a) and the mean FTLEs of $\boldsymbol{U}_1$, where the maximum in both cases is found for $\Omega = 0.5$ with relatively flat behaviour for all other frequencies. The second is that there are more unstable directions for $\Omega = 0.5$ than for all other frequencies. Hence, it seems plausible that the increased propensity to hydrodynamic instability for $\Omega = 0.5$ could lead to a more chaotic flow.

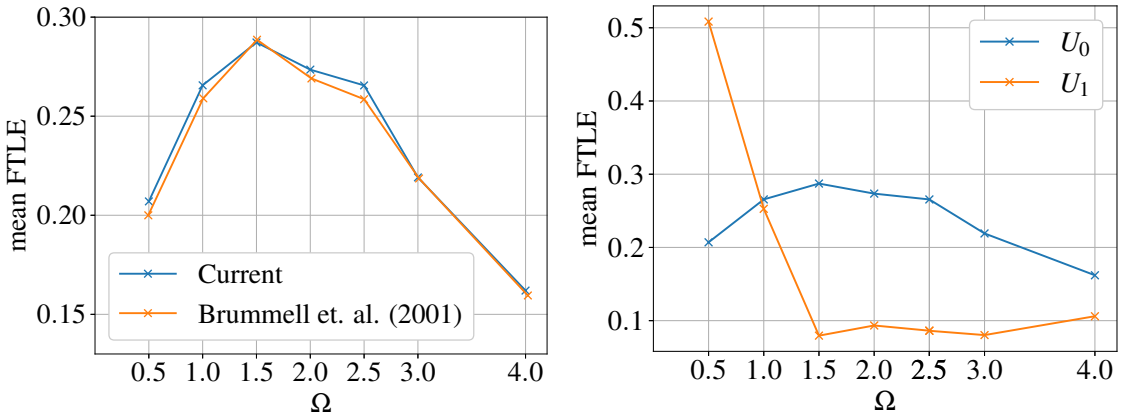

(a) Mean FTLEs for $\boldsymbol{U}_0$ using an MHD code in the kinematic regime with $R_m = 100$. Also shown are the results of Brummell *et al.* [9] for comparison.

(b) Mean FTLEs for $\boldsymbol{U}_1$ calculated with a purely hydrodynamic simulation. The results for $\boldsymbol{U}_0$ are also shown.

FIG. 8: Mean FTLEs for $\boldsymbol{U}_0$ and $\boldsymbol{U}_1$ for a range of values of Ω and $\epsilon = 1$ at $Re = 100$.

Before moving on to cases with a magnetic field present, we examine the structure of the FTLEs on the plane $z = 0$ for our two hydrodynamic states. Given that we have just shown that the FTLEs do not differ significantly from purely kinematic results in which the flow $\boldsymbol{U}_0$ is specified we present results for $\boldsymbol{U}_0$, obtained from a code that fixes the velocity field, at a higher resolution than is feasible for our other cases in figure 9. The figure shows that for all frequencies the flow is quite chaotic with very few integrable patches (indicated by dark regions). We note that the ridges present in these figures are related to Lagrangian coherent structures, and act as barriers through which particle paths do not cross [20, 21].

The FTLEs for $\boldsymbol{U}_1$ are displayed in figure 10. It is immediately clear that the Lagrangian statistics are quite different to that of $\boldsymbol{U}_0$. For low frequencies, in which the mean FTLEs increase or remain similar, we see that the flow remains chaotic nearly everywhere. This is especially evident for $\Omega = 0.5$ which shows very little areas of integrability. However, for the frequencies where the mean FTLEs decrease the areas of integrability are substantially larger, with thin ridges separating them. These changes from $\boldsymbol{U}_0$ reflected in the structure, and mean, of the FTLEs shows that as for $\boldsymbol{U}_0$ there is a clear link between the FTLEs and the magnetic energy growth rates for $\boldsymbol{U}_1$ (discussed in III B).

It is important to note that, although the FTLE for $\Omega = 0.5$ is higher for $\boldsymbol{U}_1$ than $\boldsymbol{U}_0$, the growth

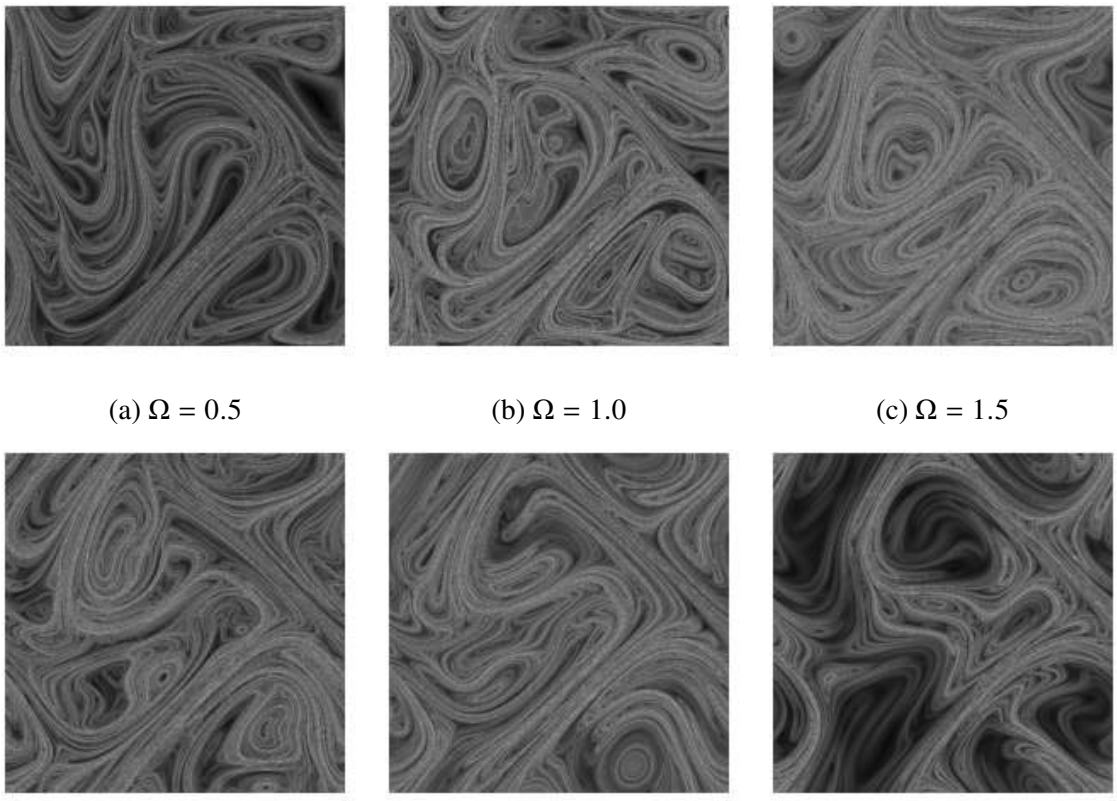

(a) $\Omega = 0.5$ (b) $\Omega = 1.0$ (c) $\Omega = 1.5$

(d) $\Omega = 2.0$ (e) $\Omega = 2.5$ (f) $\Omega = 4.0$

FIG. 9: FTLEs in the kinematic regime with $\epsilon = 1$. A greyscale colour map is used, with a FTLE of zero being black and the maximum FTLE being white. Movies of their evolution over one period are available as supplementary material.

rate is smaller. This reminds us that care is needed when interpreting the FTLEs, and that formally the link between the growth rate of a magnetic field and the FTLEs is obtained for $R_m \to \infty$. However, for $\boldsymbol{U}_0$ we see from our Floquet results that it may be a quick dynamo, setting into this asymptotic fast dynamo behaviour at our current parameters. Therefore, the discrepancy for $\boldsymbol{U}_1$ suggests that we have simply not reached this asymptotic behaviour (if in fact it exists).

With the hydrodynamic behaviour discussed, let us turn our attention to cases in which a magnetic field is present. For $R_m = 100$ section III B showed that, unlike for $R_m = 120$, not all frequencies have a region in which a non-linear dynamo is sustained. Therefore, we calculate the FTLEs starting from states at a few points in the region where the kinematic growth phase has ended, but before the eventual decay of the magnetic field. For $R_m = 120$ a non-linear dynamo is sustained at all frequencies, hence we start the FTLE calculation from a representative state in the

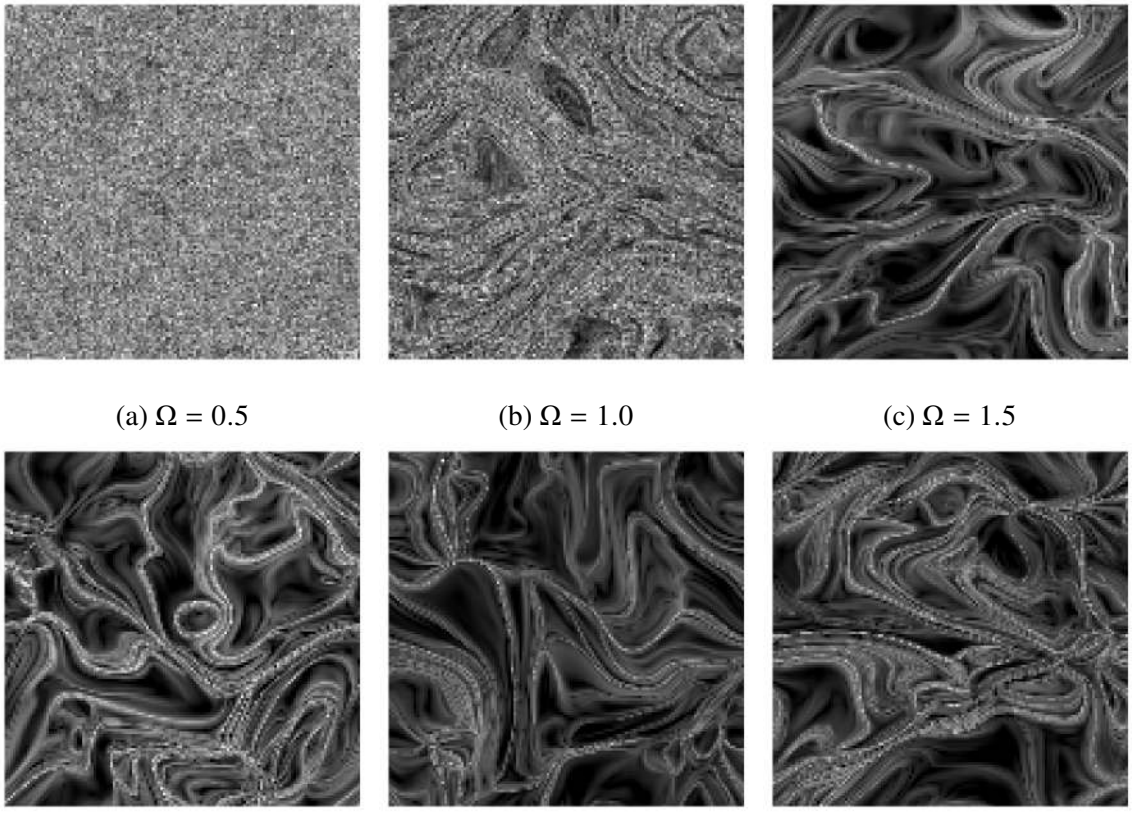

(a) $\Omega = 0.5$ (b) $\Omega = 1.0$ (c) $\Omega = 1.5$

(d) $\Omega = 2.0$ (e) $\Omega = 2.5$ (f) $\Omega = 4.0$

FIG. 10: FTLEs for $\boldsymbol{U}_1$ with $Re = 100$ and $\epsilon = 1$. A greyscale colour map is used, with a FTLE of zero being black and the maximum FTLE being white.

non-linear regime.

Figures 11a and 11b show the mean FTLE for $R_m = 100$ and $R_m = 120$, respectively. From figure 11a we see that the mean FTLE does not depend strongly on the state at which the calculation is started. The slight variations can therefore be mainly attributed to the natural slight variation that can be expected when starting the FTLE calculation from a different point of the attractor. For low frequencies the mean FTLE of the non-linear state is different from that of $\boldsymbol{U}_1$ (shown on figure 11b). This indicates that the Lorentz force is large enough that is has significantly altered the flow field form its $\boldsymbol{U}_1$ form. However, for higher frequencies the mean FTLEs are close to that of $\boldsymbol{U}_1$ showing that no such flow modification is taking place, leading to the eventual decay of the magnetic field.

For $R_m = 120$ we see from figure 11b a similar pattern to that obtained for $R_m = 100$. It is clear that for $\Omega = 0.5$ and $\Omega = 1.0$ that the Lorentz force is significantly altering the flow field, leading

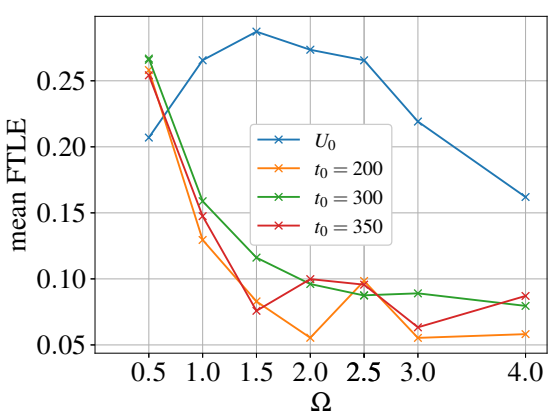

(a) Mean FTLEs for the non-linear regime at $R_m = 100$.

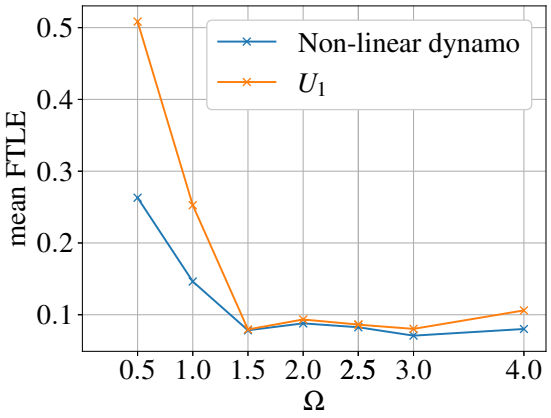

(b) Mean FTLEs for the non-linear regime at $R_m = 120$.

FIG. 11: Mean FTLEs for a range of frequencies with $Re = 100$ and $\epsilon = 1$.

to lower FTLEs, and a less chaotic flow in the non-linear dynamo regime. However, for higher frequencies there is an overall agreement for the mean FTLE in the non-linear regime, and for the hydrodynamic state $\boldsymbol{U}_1$. As in these cases the flow remains a non-linear dynamo, despite not significantly modifying the purely hydrodynamic flow, it is reasonable to suspect that the marginal instability of $\boldsymbol{U}_1$ to magnetic perturbations (shown in section III B) is partially responsible for its saturation. The FTLEs for $R_m = 120$ on the plane $z = 0$ are shown in figure 12. These FTLE images support the findings of the mean FTLEs, namely that for $\Omega = 0.5$ and $\Omega = 1.0$ the flow is less chaotic than $\boldsymbol{U}_1$ (see figure 10), but has no noticeable difference from $\boldsymbol{U}_1$ for other frequencies.

In order to provide clearer evidence for whether the magnetic field is altering the FTLEs we can consider the probability density functions (PDFs) of the FTLEs. For this purpose we consider two frequencies; $\Omega = 0.5$, for which the mean FTLE is altered, and $\Omega = 2.5$ which shows little difference. For both frequencies a normal distribution is found to be a good fit, with the resulting PDFs shown in figure 13. For $\Omega = 0.5$, figure 13a shows that there us a clear difference in the distribution of the FTLEs between $\boldsymbol{U}_0$ and $\boldsymbol{U}_1$, with the flow becoming more chaotic in $\boldsymbol{U}_1$ and any integrable regions present for $\boldsymbol{U}_0$ disappearing. Importantly we see that the distribution for the non-linear dynamo is between that of $\boldsymbol{U}_0$ and $\boldsymbol{U}_1$. Therefore, it is clear that the Lorentz force is playing a major role in this case, preventing the emergence of a $\boldsymbol{U}_1$-type flow, and modifying the velocity field to an overall less chaotic one (than $\boldsymbol{U}_1$ — though this is still more chaotic than $\boldsymbol{U}_0$).

Conversely, figure 13b shows seemingly identical distributions for $\boldsymbol{U}_1$ and the non-linear dynamo

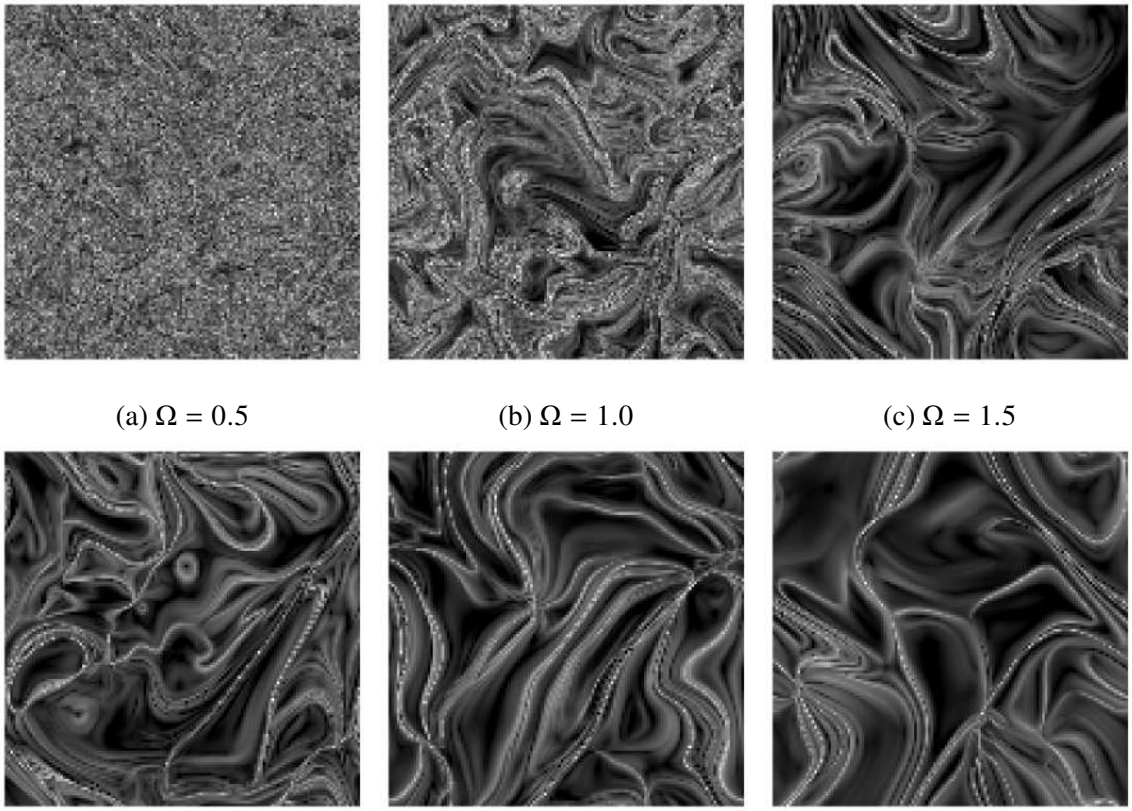

(a) $\Omega = 0.5$ (b) $\Omega = 1.0$ (c) $\Omega = 1.5$

(d) $\Omega = 2.0$ (e) $\Omega = 2.5$ (f) $\Omega = 4.0$

FIG. 12: FTLEs in the non-linear regime with $Re = 100$, $Re = 120$, and $\epsilon = 1$. A greyscale colour map is used, with a FTLE of zero being black and the maximum FTLE being white.

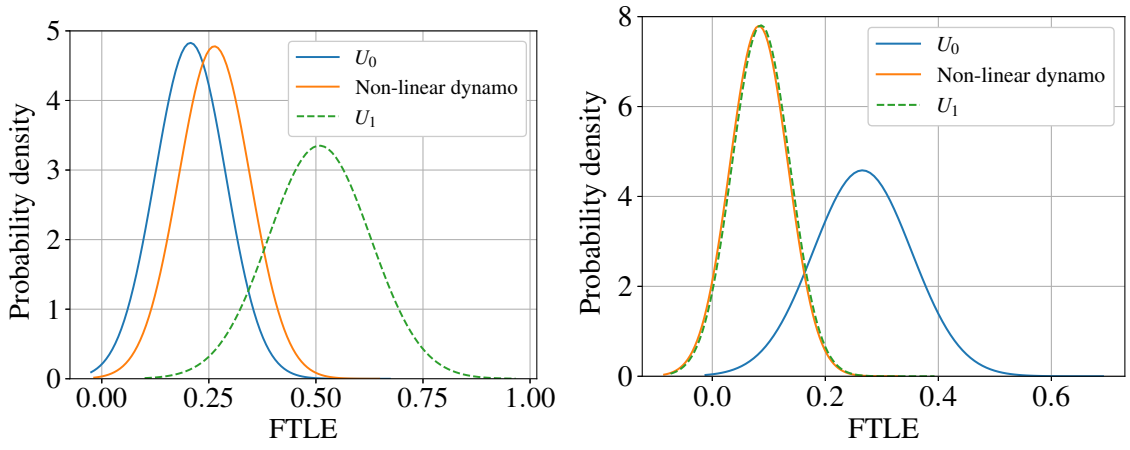

(a) $\Omega = 0.5$ (b) $\Omega = 2.5$

FIG. 13: Probability density function of the FTLEs at $R_m = 120$.

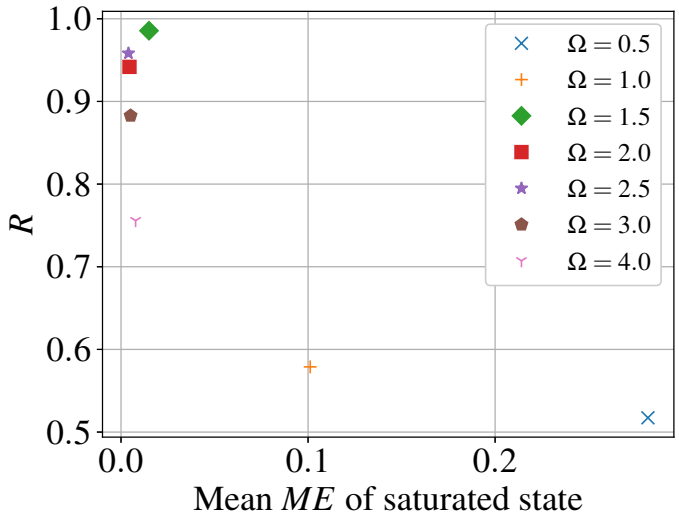

FIG. 14: The ratio of the mean FTLE of the non-linear dynamo for $R_m = 120$ to the mean FTLE of the $\boldsymbol{U}_1$ state (R) vs the mean ME of the saturated solution.

regime. This supports the hypothesis that the Lorentz force is doing very little to modify the velocity field for $\Omega = 2.5$. The reason then for saturation of the dynamo can mainly be attributed to the marginal (almost neutral) instability to magnetic perturbations properties of $\boldsymbol{U}_1$ at $\Omega = 2.5$. Therefore, even though the magnetic field must influence the velocity field to saturate, it need only do so very weakly and on long time scales. Hence, the non-linear dynamo regime can have a velocity field that remains close to $\boldsymbol{U}_1$. In general, figure 14 illustrates that the mean field strength of the dynamo is anti-correlated with the agreement between the mean FTLEs of the non-linear dynamo and the hydrodynamic state $\boldsymbol{U}_1$. This indicates that the frequencies at which the magnetic field strength is lower ($\Omega \geq 1.5$) are the same as those for which the non-linear dynamo has the same chaotic properties as $\boldsymbol{U}_1$.

D. Passive kinematic dynamo

We conclude the results by examining the stability properties of a passive vector field, governed by equation (16). By timestepping this passive dynamo in the flow-field of the non-linear dynamo regime, we can see whether the flow field remains able to amplify a kinematic vector field despite dynamo saturation. The evolution of $\boldsymbol{Z}$ starting from a small random initial condition is shown in figure 15. From figure 15a we see that only $\Omega = 0.5$ has a significantly positive growth, with all other cases being only slightly positive or negative. This is further highlighted by the

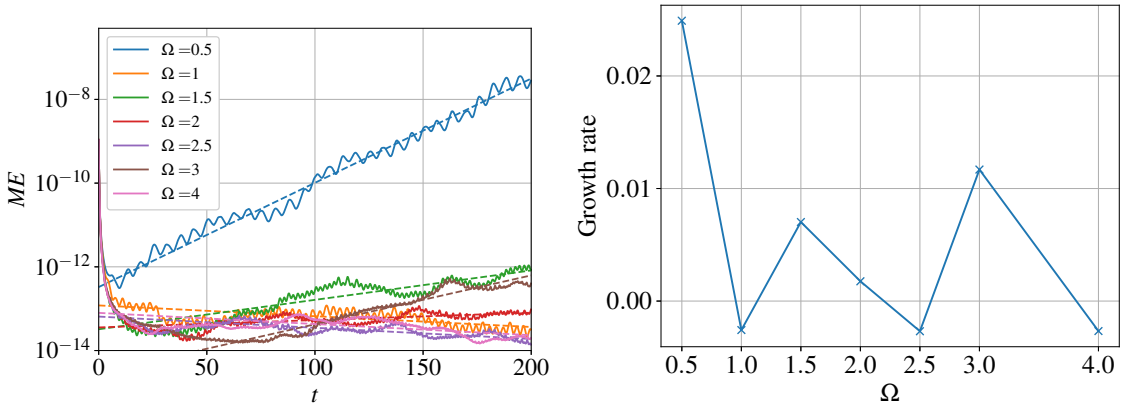

(a) Magnetic energy evolution for a range of frequencies Ω.

(b) Growth rates obtained by linear regression of the magnetic energy time series (shown as dotted lines in (a).

FIG. 15: Magnetic energy evolution and growth rates for a passive kinematic dynamo $\boldsymbol{Z}$ in the non-linear regime for $R_m = 120$.

growth rates illustrated in 15b. From these results we can see that, as in [4], the flow field from a saturated non-linear dynamo can remain a kinematic dynamo. The reason for this can be related to the correspondence between the growth rates of figure 15b, and the mean FTLEs (figure 11b), again highlighting the link between the FTLEs of a flow field, and the kinematic growth rate of a magnetic field as conjectured by Cattaneo and Tobias [4]. Hence, calculating the evolution of a passive vector field is a good proxy for a full Lagrangian calculation.

As for $\Omega = 0.5$ the passive scalar dynamo is unstable, it shows that the form of the magnetic field and its link the the velocity field is crucial in providing saturation in this case. In other words, although kinematic growth is possible as suggested by the FTLEs, non-linear growth is not due to the way in which the velocity and magnetic fields non-linearly interact. Hence it can be thought that for non-linear regimes with more chaotic properties, non-linearity is crucial in providing saturation, and the flow field must be significantly modified via the Lorentz force. For the other frequencies the growth rate is smaller and we should not read too much into their exact values. Indeed, the results of section III B show that very small growth rates for the magnetic field are possible on a time-scale not considered for the passive dynamo. Instead, as the flow remains close to $\boldsymbol{U}_1$, we should expect that the passive scalar dynamo, although eventually increasing as it should for $\boldsymbol{U}_1$ (figure 7), can have local periods of stability as shown in figure 15b. These local

areas of stability could result from a weak Lorentz force and are enough to saturate the flow.

IV. CONCLUSION

In this paper we have revisited the dynamo properties of a class of periodic (in space) oscillatory dynamo flows, for a range of oscillation frequencies and fluids and magnetic Reynolds numbers. We have calculated the stability of such flows, both to hydrodynamic and magnetic perturbations using a Floquet analysis. Furthermore, we have examined the Lagrangian stretching properties of the kinematic and saturated dynamo flows, using a particle tracking method that enables the calculation (in the open source software Dedalus) of the finite-time Lyapunov exponents (FTLEs) [17]. We find that, depending on the frequency of oscillation, the stretching in the saturated state as measured by the average FTLE may increase or (more usually) decrease. The distribution of FTLEs remains well-approximated by a normal distribution in the saturated regime though the mean and variance of this distribution is modified by the presence of the magnetic field.

We further demonstrate that the calculation of the evolution of a passive vector field gives a very good proxy for a full Lagrangian calculation, validating the approach taken by Cattaneo and Tobias [4]. Interestingly Cattaneo and Tobias [4] found cases in both convecting systems and forced shell models where the growth-rate of a passively stretched vector field for a saturated dynamo state *increased* from that for the hydrodynamic velocity field. This was the case for a subset of the forced models considered here — confirmed via calculation of the FTLEs. Hence it is not simple to predict *a priori* whether the presence of a magnetic field in the saturated state will lead to the diminution of chaos. It remains an interesting avenue for future investigation when the structure of dynamo flows and the generated magnetic field does lead to a system with increased stretching and chaos.

There are certainly systems where such an increase in chaos and turbulence is believed to be significant. For example in “essentially nonlinear" dynamos, a finite amplitude magnetic field can lead to the onset of turbulence and hence chaotic stretching. Such dynamos are often subcritical and we conjecture that subcriticality may sometimes be associated with an increase of chaotic stretching imparted by the change in stability provided by a finite amplitude magnetic field.

Finally, we note that the Floquet analysis we perform here about the hydrodynamic state is particularly simple, as it separates into two independent classes of modes. The case of Floquet analysis about a saturated MHD state is more complicated. This case is relevant to determining the stability of saturated MHD states to long wavelength instabilities, and hence the important problem

of the generation of large scale magnetic field from a fully saturated small-scale dynamo.

ACKNOWLEDGMENTS

This work was undertaken on ARC4, part of the High Performance Computing facilities at the University of Leeds, UK. We acknowledge partial support from a grant from the Simons Foundation (Grant No. 662962, GF). We would also like to acknowledge support of funding from the European Union Horizon 2020 research and innovation programme (grant agreement no. D5S-DLV-786780). Additionally, we would like to thank the Isaac Newton Institute for Mathematical Sciences, Cambridge, for support and hospitality during the programme DYT2 where work on this paper was undertaken. This work was supported by EPSRC grant no EP/R014604/1.

---

[1] K. Moffatt and E. Dormy, *Self-Exciting Fluid Dynamos*, Cambridge Texts in Applied Mathematics (Cambridge University Press, 2019).

[2] I. Klapper and L. S. Young, Rigorous bounds on the fast dynamo growth-rate involving topological entropy, Comm. Math. Phys. **175**, 623 (1995).

[3] J. M. Finn and E. Ott, Chaotic flows and fast magnetic dynamos, Physics of Fluids **31**, 2992 (1988).

[4] F. Cattaneo and S. M. Tobias, Dynamo properties of the turbulent velocity field of a saturated dynamo, Journal of Fluid Mechanics **621**, 205 (2009).

[5] F. Cattaneo, D. W. Hughes, and E.-J. Kim, Suppression of chaos in a simplified nonlinear dynamo model, Physical Review Letters **76**, 2057 (1996).

[6] E. Zienicke, H. Politano, and A. Pouquet, Variable Intensity of Lagrangian Chaos in the Nonlinear Dynamo Problem, Phys. Rev. Lett. **81**, 4640 (1998).

[7] E. L. Rempel, A. C-L Chian, and A. Brandenburg, Lagrangian chaos in an ABC-forced nonlinear dynamo, Physica Scripta **86**, 018405 (2012).

[8] H. Homann, Y. Ponty, G. Krstulovic, and R. Grauer, Structures and Lagrangian statistics of the Taylor-Green dynamo, New Journal of Physics **16**, 075014 (2014).

[9] N. H. Brummell, F. Cattaneo, and S. M. Tobias, Linear and nonlinear dynamo properties of time-dependent ABC flows, Fluid Dynamics Research **28**, 237 (2001).

[10] B. Galanti, A. Pouquet, and P. Sulem, Influence of the period of an ABC flow on its dynamo action, in *Solar and Planetary Dynamos*, Publications of the Newton Institute, edited by M. R. E. Proctor, P. C.

Matthews, and A. M. Rucklidge (Cambridge University Press, 1994) p. 99?104.

[11] G. Floquet, Sur les équations différentielles linéaires à coefficients périodiques, Annales scientifiques de l'École Normale Supérieure **12**, 47 (1883).

[12] K. J. Burns, G. M. Vasil, J. S. Oishi, D. Lecoanet, and B. P. Brown, Dedalus: A flexible framework for numerical simulations with spectral methods, Phys. Rev. Research **2**, 023068 (2020).

[13] S. M. Tobias, The turbulent dynamo, Journal of Fluid Mechanics **912**, P1 (2021).

[14] D. Barkley and R. D. Henderson, Three-dimensional Floquet stability analysis of the wake of a circular cylinder, Journal of Fluid Mechanics **322**, 215 (1996).

[15] A. M. Soward, Fast dynamos, in *Lectures on Solar and Planetary Dynamos*, Publications of the Newton Institute, edited by M. R. E. Proctor and A. D. Gilbert (Cambridge University Press, 1994) pp. 181–218.

[16] S. G. Llewellyn Smith and S. M. Tobias, Vortex dynamos, Journal of Fluid Mechanics **498**, 1 (2004).

[17] C. S. Skene and S. M. Tobias, csskene/ABC-dynamo_FTLE: Initial release, https://doi.org/10.5281/zenodo.7565686 (2023).

[18] S. M. Tobias and F. Cattaneo, Dynamo action in complex flows: the quick and the fast, Journal of Fluid Mechanics **601**, 101 (2008).

[19] I. Bouya and E. Dormy, Toward an asymptotic behaviour of the ABC dynamo, EPL (Europhysics Letters) **110** (2015).

[20] G. Haller, Lagrangian coherent structures from approximate velocity data, Physics of Fluids **14**, 1851 (2002).

[21] S. C. Shadden, F. Lekien, and J. E. Marsden, Definition and properties of Lagrangian coherent structures from finite-time Lyapunov exponents in two-dimensional aperiodic flows, Physica D: Nonlinear Phenomena **212**, 271 (2005).